

D/H in a new Lyman Limit Absorption System at $z = 3.256$ towards PKS1937-1009

N. H. M. Crighton¹*, J. K. Webb¹, A. Ortiz-Gill², A. Fernàndez-Soto²

¹ School of Physics, University of New South Wales, Sydney NSW 2052, Australia

² Observatori Astronòmic, Universitat de València, Burjassot (València), E-46100, Spain

ABSTRACT

We have identified a new Lyman limit absorption system towards PKS1937-1009, with $\log N(\text{H}\text{I}) = 18.25 \pm 0.02$ at $z = 3.256$. It is suitable for measuring D/H, and we find a 68.3% confidence range for D/H of $1.6_{-0.30}^{+0.25} \times 10^{-5}$, and a 95.4% range of $1.6_{-0.4}^{+0.5} \times 10^{-5}$. The metallicity of the cloud where D/H was measured is low, $[\text{Si}/\text{H}] = -2.0 \pm 0.5$. At these metallicities we expect that D/H will be close to the primordial value. Our D/H disagrees at a level of 99.4% with the predicted D/H using the Ω_b calculated from the cosmic background radiation measured by WMAP, $2.60_{-0.17}^{+0.19} \times 10^{-5}$. Our result also exacerbates the scatter in D/H values around the mean primordial D/H.

Key words: nuclear reactions, nucleosynthesis, abundances - quasars: absorption lines - cosmological parameters.

1 INTRODUCTION

There are interesting disagreements between the various ways of calculating the baryon density of the universe (Ω_b). The most precise Ω_b measurement is from the recent WMAP observations of the CMB power spectrum (Spergel et al. 2003). Another way to measure Ω_b is by measuring the relative abundances of the light elements produced in BBN. Attempts have been made to measure the primordial He^4 , Li^7 and deuterium (D) abundances. In principle, Ω_b is most reliably determined by D, due to its apparently uncomplicated evolution with time (Epstein, Lattimer & Schramm 1974) and that it depends more sensitively on Ω_b than He^4 and Li^7 . There is broad agreement between the D Ω_b and CMB Ω_b , but the He^4 and Li^7 measurements predict a lower Ω_b . Either there is something wrong with our interpretation of the He^4 and Li^7 measurements, or our understanding of BBN.

The mean of the primordial deuterium values as measured in quasar absorption systems is consistent with the WMAP CMB Ω_b . However, there is statistically significant scatter of the individual D/H measurements about the mean. The metallicity of the absorption clouds used to make the D/H measurements is low, $[\text{M}/\text{H}] < -1.5$, so that no astrophysical (deuterium destruction due to stellar nucleosynthesis) is thought to have occurred (Fields 1996). In addition,

the primordial D/H is thought to be isotropic and homogeneous, so the scatter is hard to explain. One explanation is that the systematic errors in measuring D/H have been underestimated by the authors. However, with only five measurements (Burles & Tytler 1998a,b; O'Meara et al. 2001; Pettini & Bowen 2001; Levshakov et al. 2002), other explanations, such as some early mechanism for astrophysics or a non standard BBN, cannot be ruled out. More D/H measurements are needed to resolve this problem. It is exciting to see further results being added to this short list: recently two further D/H measurements have been published: one towards another QSO absorption line system (Kirkman et al. 2003) and another in a low metallicity gas cloud near our Galaxy (Sembach et al. 2004).

Here we present an analysis of D/H in a newly discovered $z = 3.256$ absorption system towards PKS1937-1009 (see Fig. 1). Coincidentally, Burles & Tytler (1998a) measured D/H in a different absorber at $z = 3.572$ towards this same QSO. The new absorber is not connected with the $z = 3.572$ absorber, and we expect it to give an independent measurement of D/H.

2 OBSERVATIONS

PKS1937-1009 was first identified as a quasar with $z_{\text{em}} = 3.787$ by Lanzetta et al. (1991). Our observations of PKS1937-1009 were taken on Keck I with the HIRES and LRES instruments. The LRES observations were taken on

* E-mail: nhmc@phys.unsw.edu.au

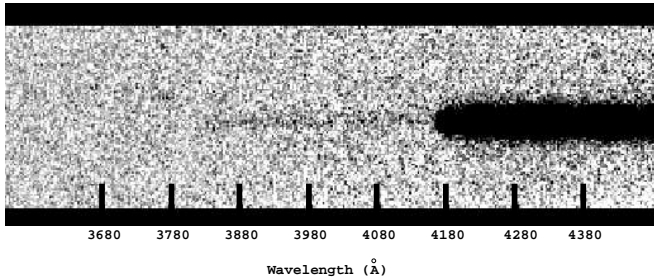


Figure 1. The two dimensional LRES spectrum, showing the position of the $z = 3.572$ LL at ~ 4170 Å. The LL due to the $z = 3.256$ system we are interested in can be seen at ~ 3880 Å.

9th August, 1996 and the HIRES observations were taken over the 31st May and 1st June, 1997. The HIRES spectrum was taken using the C5 decker, giving a resolution of 8.8 km s^{-1} FWHM. The LRES spectra were taken using the 300/5000 grating, giving a resolution of ~ 7.4 Å FWHM.

The data reduction was carried out using standard IRAF routines. The raw CCD frames were flat fielded and ADU counts corrected to photon counts. Medians were formed of the 2D images to eliminate most of the cosmic rays. An observation of a standard star was used to trace the spectra in the 2D CCD image (for both LRES and HIRES data) and that trace was adopted in carrying out the extraction from 2D to 1D spectra. The stellar trace was applied to the quasar exposures, allowing it to translate in the spatial direction to account for shifts between the relative placing of the quasar and star along the spectrograph slit. Optimal extraction was done, using the weights derived from the standard star spectrum. Error arrays were propagated throughout the extraction procedure. Polynomials were fitted to ThAr lamp exposures to relate pixel number to wavelength. We checked for shifts between calibration exposures bracketing the quasar observations and time-interpolated where necessary. The wavelength scales were corrected to a heliocentric reference frame and all spectra were rebinned onto a linear wavelength scale.

The LRES spectra were flux calibrated using the standard star observations to recover the correct underlying spectral shape of the quasar continuum. No flux calibration was applied to the HIRES spectra. The final HIRES spectrum covers wavelengths from 4100 – 6400 Å with a signal to noise ratio (S/N) per pixel of 20 at 5000 Å. The LRES spectrum covers the range 3700 – 7400 Å, with a S/N per pixel of ~ 200 at 6000 Å.

3 ANALYSIS

We fit Voigt profiles to the relevant absorption lines using the program VPFIT¹. This uses a χ^2 minimisation procedure to find the best fitting redshift, column density (cm^{-2}) and b parameter ($b = \sqrt{\sigma}$) for each absorption line. The diagonals of the covariance matrix give the error estimates on each of the fitted parameters. These errors assume that the χ^2 parameter space around the best fitting solution is parabolic, which is not always the case. In particular, if there

are degeneracies in the fitted parameters, the χ^2 parameter space needs to be explicitly explored to find the correct error ranges (see Crighton et al. (2003)). For the majority of the transitions we fit in the $z = 3.256$ system, the errors given by the covariance matrix are sufficiently accurate. However, to find the errors on the best fitting value of D/H, we do not use the errors given by VPFIT, but instead explicitly calculate χ^2 as a function of D/H, as described in section 3.9.

3.1 Absorption lines present in the $z = 3.256$ system

\mathfrak{Z} (1334), Si II (1260) and Si IV (1393 and 1402) (Fig. 3), H I Ly α and Ly β (Fig. 4) transitions are present at $z = 3.256$ in the HIRES spectrum. There is a narrow line in the blue wing of the H I Ly α line which we believe is D I. The $z = 3.256$ Lyman limit (LL) is present in the LRES spectrum (Fig. 2). All higher order H I transitions are at wavelengths shorter than the LL due to the higher redshift absorber at $z = 3.572$, and cannot be detected in our HIRES spectrum.

The HIRES spectrum covers the position of Si III (1206.5) and Fe II (1144), but they are blended with H I absorption in such a way that no useful constraints are possible.

Both the Si II and \mathfrak{Z} lines fall in the Ly α forest, where there is the danger that an H I forest line may be misidentified as a metal line. However, we are confident that we have correctly identified Si II and \mathfrak{Z} for two reasons. Firstly, their widths are much smaller than expected for the average Ly α forest H I line. Secondly, they fall within a few km s^{-1} of the expected redshift based on $z(\text{H I})$ and $z(\text{Si IV})$. Unfortunately, both Si II and \mathfrak{Z} lines are to some extent blended with H I Ly α absorption, which may be hiding weaker Si II and \mathfrak{Z} components.

The Si IV lines are at wavelengths longer than the quasar H I Ly α emission and so are not blended with forest lines.

The \mathfrak{Z} and Si II appear to be at the same redshift, $z(\mathfrak{Z}) = 3.256009 \pm 0.000006$ and $z(\text{Si II}) = 3.256001 \pm 0.000009$.

There are three Si IV components, one main component at $+3.4 \pm 0.4$ km s^{-1} (redward) relative to the \mathfrak{Z} position, and two lower column density components at $+21.4 \pm 0.7$ km s^{-1} and $+43.4 \pm 0.7$ km s^{-1} .

The metal line parameters and their errors are given in Table 2.

3.2 H I column density

The $z = 3.256$ Lyman limit is optically thick, so there is a lower limit on the total $\log N(\text{H I})$ of ~ 17.6 . There are also damping wings at the Ly α line, which further constrains $N(\text{H I})$ (Fig. 5). Other things could explain these damping wings; perhaps the continuum dips over the Ly α line, due to two emission lines on either side of the Ly α line. However, composite qso spectra [e.g. Vanden Berk et al. (2001)] display no emission lines associated with the quasar redshift at the relevant wavelengths to cause this apparent dip in the continuum. We believe our two estimates of the continuum, described below, adequately account for any uncertainty in the shape of the continuum.

¹ Carswell et al., <http://www.ast.cam.ac.uk/~rfc/vpfit.html>

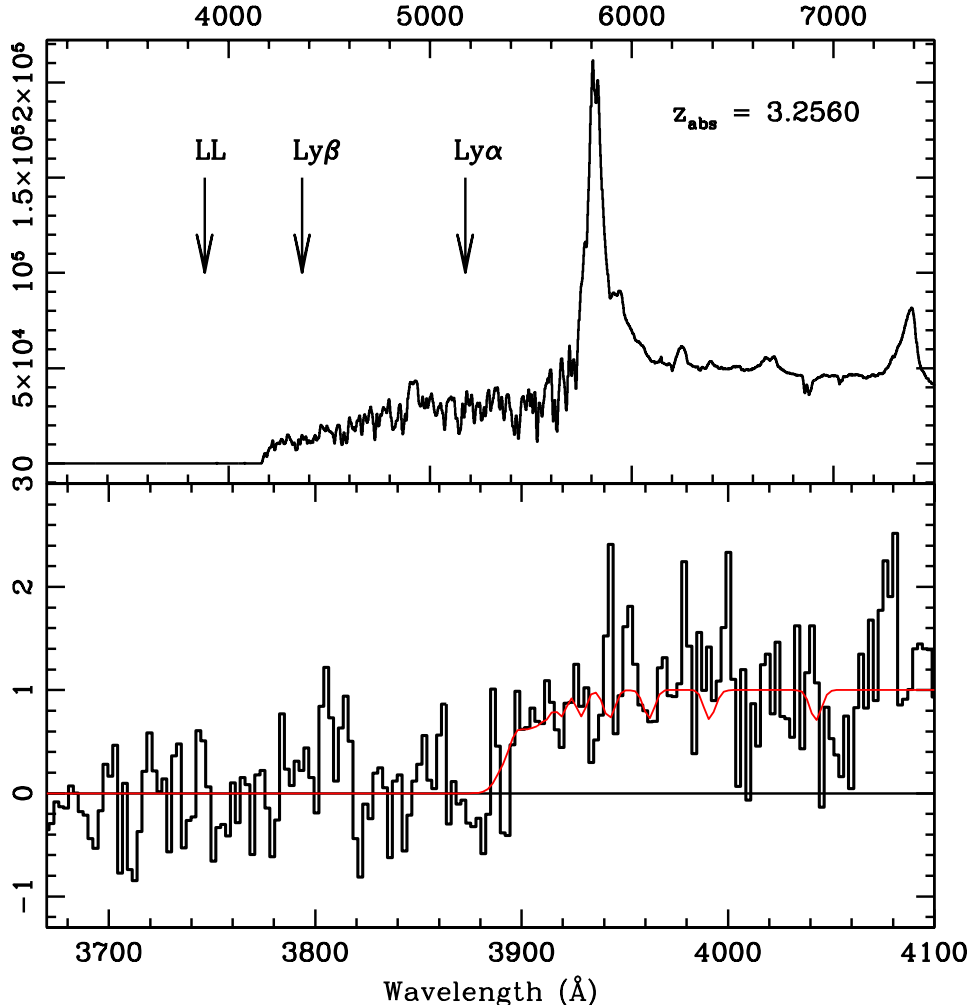


Figure 2. The entire LRES spectrum (above) and an expanded region of the spectrum showing the LL due to the $z = 3.256$ absorber (below). The fit corresponding to model (2d) (see section 3.3) is shown in the expanded spectrum.

Table 1. The absorption line parameters and their errors, found using from the diagonals of the covariance matrix in VPFIT, for \mathfrak{Z} , Si II and the three Si IV components.

Ion	$\log(N)$ (cm^{-2})	z	b (km s^{-1})
\mathfrak{Z}	13.600 ± 0.045	3.256009 ± 0.000006	6.9 ± 0.7
Si II	12.875 ± 0.093	3.256001 ± 0.000009	5.0 ± 1.4
Si IV	12.820 ± 0.011	3.256057 ± 0.000002	6.5 ± 0.3
Si IV	12.138 ± 0.039	3.256303 ± 0.000005	1.3 ± 1.3
Si IV	11.970 ± 0.036	3.256626 ± 0.000006	2.8 ± 1.3

3.3 Continuum placement

To generate the continuum we fitted regions that were apparently free from absorption around each absorption feature, with low order Chebyshev polynomials. The damping wings present in the H I Ly α line provide the best constraint on the total $N(\text{H I})$, but the derived $N(\text{H I})$ value is sensitive to the placement and shape of the continuum above the damping wings. To take this into account, we fitted two different continua above the Ly α line using 2nd and 3rd or-

der Chebyshev polynomials. We also allow the continuum to vary above the Ly α and Ly β lines by multiplying it by a parameter, initially set to 1, which is allowed to vary during the χ^2 minimisation.

3.4 H I velocity structure

We try to determine the velocity structure in two ways: firstly, by fitting the available H I transitions with as few components needed to obtain an acceptable fit, and sec-

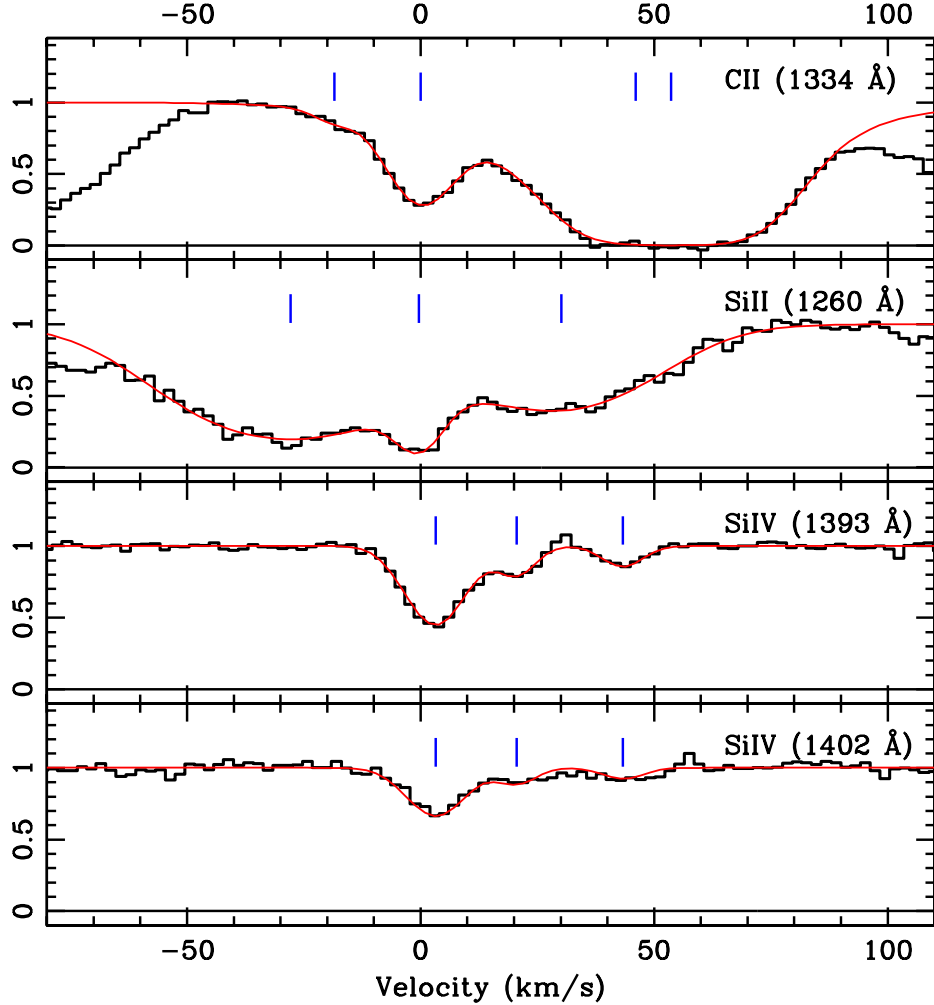


Figure 3. The ζ , SiII and SiIV lines along with their best fitting models used to derive the parameters found in table 2. The velocity zero point is the redshift of the ζ line, $z = 3.256009$. The histogram shows the data and the curves show the fitted model. The absorption lines away from the $v = 0$ position in the top two panels are due to Ly α forest lines. The three components in the bottom two panels are all due to SiIV.

ondly, by looking at the metal lines to indicate the possible position of H α components. Ideally we would like to fit many higher order H α Lyman transitions to help determine the velocity structure, but only the Ly α and Ly β lines are available.

A single H α component cannot satisfactorily fit both the Ly α and Ly β lines, so at least two components are present.

We expect at least four hydrogen components, one at $z(\zeta)$ and three corresponding to the SiIV component positions. However, we don't know what H α column density is associated with each one. We expect the ζ and SiII components to have a greater proportion of their associated H gas in the form of H α , as their ionization potentials are close to that of H α . Therefore, if there is no significant metallicity variation across the absorption complex, an H α component near $z(\zeta)$ is likely to be the dominant component in the Ly α and Ly β line.

Below we describe the velocity models we explored.

3.4.1 Model (1): two H α components, $z(H\alpha)$ tied to $z(\zeta)$

We initially assemble a model using two H α components, with the redshift of the bluer component tied to the ζ redshift. In this fit we include D α components for both H α components. We tie the redshifts of corresponding D α and H α components together, and fit a single D/H to both components (we discuss this assumption in section 3.8). Since the redder D α component is heavily blended with the bluer H α component, we tie its b parameter to the b parameter of the corresponding H α component, assuming purely thermal broadening (this assumption has no effect on the final D/H value; see section 3.6). We fit the summed total of the H α column density of both components, instead of individually fitting the column densities of each component. We do this because while the column density in each component is not well constrained, the total log $N(H\alpha)$ is. This model does not fit the D α line in the Ly α line adequately. We can obtain an acceptable fit if we include very weak absorption from some unknown contaminating metal line near the D α posi-

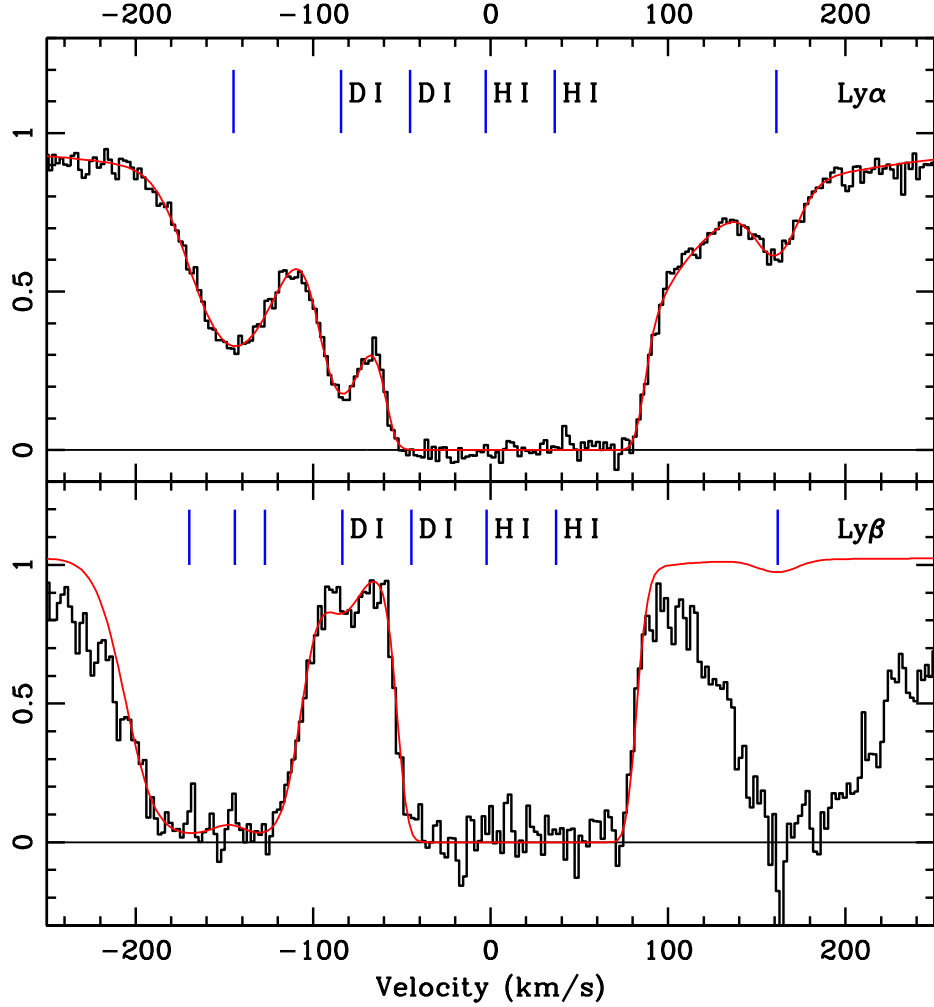


Figure 4. The Ly α and Ly β lines, along with a fit to data. The fit corresponds to model (2d), a two H I component fit where the level of the continuum is allowed to vary above both the Ly α and Ly β lines. The continuum over the Ly α line was generated using a 3rd order chebyshev polynomial. The velocity zero point is the redshift of the β line. The histogram shows the data and the narrow curve shows the fitted model.

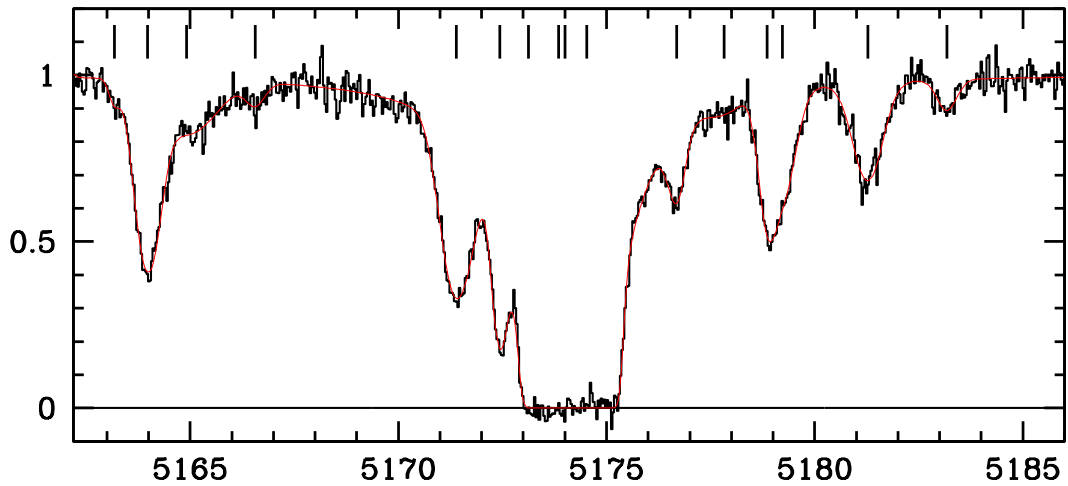


Figure 5. The Ly α line showing the damping wings and the best fitting model, model (2d). The histogram shows the data and the narrow curve shows the fitted model.

tion. However, this results in $D/H < 0.6 \times 10^{-5}$ (1σ upper limit). This is smaller than even the lowest estimates of the interstellar medium D/H , $\sim 1.0 \times 10^{-5}$ (Hébrard & Moos 2003).

3.4.2 Model (2): two $H\alpha$ components, $z(H\alpha)$ not tied to $z(\text{metals})$

It is possible that the main $H\alpha$ component does not fall at exactly the same position as the $\frac{3}{2}$ and Si II lines. This could be due to several reasons: perhaps an error in the wavelength calibration of a few km s^{-1} , or a gradient in the metallicity across the cloud. For this reason, we explore a model that does not tie the redshifts of the $H\alpha$ components to that of the metal lines. This model is identical to the model above, except it no longer ties the redshift of the bluer $H\alpha$ component to the $\frac{3}{2}$ line. This model gives an acceptable fit to the data. The position of the bluer hydrogen component is $-3.1 \pm 0.7 \text{ km s}^{-1}$ relative to $\frac{3}{2}$. The redder $H\alpha$ component is at $+40.0 \pm 1.0 \text{ km s}^{-1}$.

3.4.3 Model (3): four $H\alpha$ components, $z(H\alpha)$ tied to $z(\text{metals})$

We included four $H\alpha$ components, the redshift of each tied to a metal line component redshift (one corresponding to the $\frac{3}{2}/\text{Si II}$ position and one for each Si IV component). We include $D\alpha$ for all components where $\log N(H\alpha) > 17.0$. This does not give a satisfactory fit to the data: the narrow $D\alpha$ line in the $\text{Ly}\alpha$ line in particular is very poorly fit. As in model (1), the fit could be improved by including very weak contaminating absorption near the $D\alpha$ position. Again, this gives a low D/H , $< 0.5 \times 10^{-5}$, much lower than the ISM D/H .

Model (2) gives the only acceptable fit to the data. Models (1) and (3) can give an acceptable fit, but we need to include an unidentified metal line blended with $D\alpha$, and there is no other evidence that this is present. If we do include such a line, the measured D/H in this absorber is much smaller than the ISM D/H .

We split model (2) into four sub-models, using (2a) a 2nd order polynomial fixed continuum, (2b) a 3rd order polynomial fixed continuum, (2c) a 2nd order polynomial varying continuum and (2d) a 3rd order polynomial varying continuum.

3.4.4 Two unresolved questions about the best-fitting model

The best fitting model seems to fall below the data at -90 km s^{-1} in the $\text{Ly}\beta$ line (Fig. 4). There could be several reasons for this. It is possible that the apparent discrepancy is due to noise, or there may be a weak cosmic ray at this position that has not been completely removed. Perhaps there is a weak, narrow $\text{Ly}\alpha$ forest line near -75 km s^{-1} . However, such a line would need to have a width much smaller than the median width of forest lines. A metal line could have a narrow width, but the higher redshift system at $z = 3.572$ does not have any metal lines which fall at this position. No

other absorption systems were identified that could explain a metal line appearing at this position. We tentatively conclude that a noise spike is the cause of this discrepancy and note that it does not have a significant effect on the measured D/H , as the tightest constraint on $N(D\alpha)$ comes from the $\text{Ly}\alpha D\alpha$ line.

We would expect the Si II and $\frac{3}{2}$ redshifts to be consistent with the redshift of the $H\alpha$ line associated with them. Instead we find that the $\text{Si II}/\frac{3}{2}$ position differs from the $H\alpha$ position by $3.1 \pm 0.7 \text{ km s}^{-1}$, or about one pixel. It is possible that there are problems with the wavelength calibration. This is unlikely, however, given that the Si II and $\frac{3}{2}$ positions agree to within 1 km s^{-1} , and that the typical wavelength accuracy of a polynomial fit to an arc exposure from HIRES is better than 0.5 km s^{-1} . It is more likely that our velocity model is wrong in some way. The true velocity structure of the absorption complex will almost certainly be more complicated than our simple two component model. However, we note for all other velocity models that we considered, D/H was substantially *lower* ($< 0.6 \times 10^{-5}$) than the value that we quote for Model 2(b).

Both of these questions may be resolved by much higher S/N observations of this absorption system.

3.5 Ionization and metallicity

We have $N(\text{Si II})$ and $N(\frac{3}{2})$ in a single gas cloud, and $N(\text{Si IV})$ in three other clouds. We use the program CLOUDY (Ferland 1997) to generate an ionization model for the absorption system. When generating the model, we assume that the bluest Si IV component, the Si II and $\frac{3}{2}$ component, and the bluest $H\alpha$ component are all associated with the same gas, even though they span $\sim 6 \text{ km s}^{-1}$. We approximate the geometry of the cloud as a plane parallel slab illuminated by a distant point source and assume the proportion of metals to be solar. For calculating ionization fractions, the hydrogen particle density, n_H and the incident radiation flux on the cloud, J_ν are degenerate. Instead of specifying either n_H or J_ν , we use the parameter U :

$$U = \frac{4\pi J_{912}}{hc n_H} = 2 \times 10^{-5} \frac{J_{912}/10^{-21.5}}{n_H/(1 \text{ cm}^{-3})}$$

Here J_{912} is the incident radiation at 912 \AA , c is the speed of light and h is Planck's constant. We generate ionization models for a range of metallicities and U values, using a Haardt-Madau ionizing radiation continuum at a redshift of 3.25 (Haardt & Madau 1996). We have not explored the effect a different ionizing radiation continuum may have on the ionization fractions. $N(\text{Si II})$ and $N(\text{Si IV})$ suggest that the system has a total metallicity $[\text{Si}/\text{H}] \sim -2.0$. $N(\frac{3}{2})$ is lower than expected for this $[\text{Si}/\text{H}]$ which might indicate that C is under abundant compared to Si (see Fig. 6). This is unlikely to be due to differential dust depletion, since C has a lower condensation temperature than Si. We would expect Si, not C, to be under abundant if there is any depletion on to dust (Lu et al. 1996). With so few transitions we can only make broad generalisations about conditions in the cloud. We take a value of $[\text{Si}/\text{H}] -2.0$ with an error of ~ 0.5 dex, where this error is dominated by the uncertainty on $N(H\alpha)$ in the bluest $H\alpha$ component.

Table 2. The best fitting parameters of the lines used to fit the Ly α and Ly β lines and the LL of the $z = 3.256$ absorber. The errors are those returned by VPFIT, calculated using the diagonals of the covariance matrix. The first two H I components in the table have associated D I lines which we included. We fitted the total column density of both these components - the column density entry next to the first H I component give the value of and error on the total column density of both H I components.

Ion	$\log N$ (cm $^{-2}$)	z	b (kms $^{-1}$)
H I	18.248 ± 0.019 (total)	3.255961 ± 0.000008	15.9 ± 0.3
H I		3.256527 ± 0.000064	15.4 ± 1.4
D I	13.408 ± 0.069 (total)	3.255961 (tied to H I)	11.7 ± 0.9
D I		3.256527 (tied to H I)	10.9 (tied to H I)
H I	13.518 ± 0.015	3.253949 ± 0.000007	27.0 ± 0.8
H I	12.778 ± 0.030	3.258295 ± 0.000011	15.2 ± 1.3
H I	13.80 ± 0.17	2.589485 ± 0.000047	16.6 ± 2.8
H I	14.118 ± 0.093	2.588976 ± 0.000061	28.7 ± 5.0
H I	12.10 ± 0.17	3.259235 ± 0.000113	29.0 ± 14
H I	12.95 ± 0.34	3.260084 ± 0.000036	15.2 ± 3.3
H I	13.11 ± 0.24	3.260384 ± 0.000136	23.8 ± 6.0
H I	13.117 ± 0.014	3.262072 ± 0.000010	27.2 ± 1.0
H I	12.395 ± 0.054	3.263636 ± 0.000025	18.3 ± 2.7
H I	13.393 ± 0.038	3.247848 ± 0.000007	22.3 ± 1.1
H I	13.126 ± 0.084	3.248620 ± 0.000112	55 ± 10
H I	11.99 ± 0.13	3.247188 ± 0.000028	8.8 ± 3.5
H I	12.21 ± 0.11	3.249973 ± 0.000037	17.3 ± 4.5

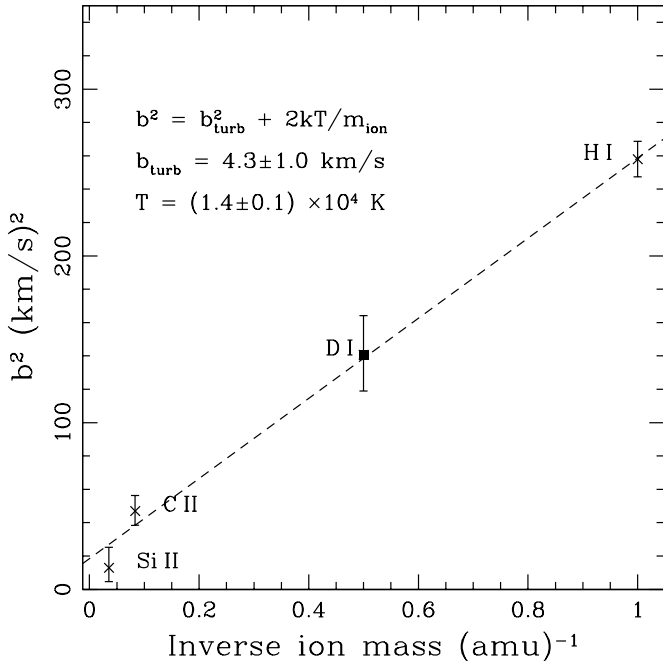


Figure 7. The b parameter squared (kms $^{-1}$) 2 versus the inverse ion mass (amu $^{-1}$). The dashed line is the least squares line of best fit to the Si II, C II, and H I points. D I is shown for comparison. The error bars in each case are calculated from the 1σ errors given by VPFIT.

3.6 b parameter test

We can predict the b parameter of the blue D I component from the b parameters of the Si II, C II and H I lines. This is done by measuring the thermal line broadening, b_{therm} , and turbulent broadening, b_{turb} , by using the b parameters from all available ions. If we assume the absorbing cloud has a thermal Maxwell-Boltzmann distribution and any turbu-

lence can be described by a Gaussian velocity distribution, then the b parameter for a particular ion will be given by

$$b_{\text{ion}}^2 = b_{\text{therm}}^2 + b_{\text{turb}}^2. \quad (1)$$

Here $b_{\text{therm}}^2 = \frac{2kT}{m}$, where T is the temperature of the gas cloud, m is the mass of the absorbing ion and k is Boltzmann's constant. b_{turb}^2 represents the Gaussian broadening due to small scale turbulence, and is the same for all ionic species. We plot b^2 against inverse ion mass in Fig. 7. Subject to the assumptions above, all the ions in the same cloud velocity space should lie on a straight line whose intercept gives b_{turb} and slope gives the cloud temperature. C II, Si II and H I all have relatively low ionization potentials (IP); 24.4, 16.3 and 13.6 eV, respectively. There is evidence from damped Ly α absorbers that even 'intermediate' IP ions, such as Al III (IP 28.4 eV), have a similar velocity structure to lower IP ions (Wolfe & Prochaska 2000). Thus we assume that the Si II and C II lines arise in the same gas as the H I and fit a least squares line of best fit to these three points. This is shown as the dashed line in Fig. 7. The D I point is plotted with its 1σ error bars as given by VPFIT. We find a temperature of $1.4 \pm 0.1 \times 10^4$ K and a turbulent broadening of 4.3 ± 1.0 kms $^{-1}$. These values suggest a b parameter for the blue D I component of 11.9 kms $^{-1}$. This is consistent with our fitted $b(DI)$ of 11.7 ± 0.9 kms $^{-1}$ for the blue D I component.

There is no way to measure the b parameter of the red D I component, since it is heavily blended with the H I blue component. We also cannot predict what $b(DI)$ will be using the method above, since we do not have any low ionization metal lines corresponding to the red H I component. In our velocity models we explored the maximum and minimum $b(DI)$ values, corresponding to purely thermal [$b(DI) = 1/\sqrt{2} b(HI)$] and purely turbulent [$b(DI) = b(HI)$] broadening. The measured D/H is not affected by which broadening we assume. Thus we arbitrarily choose pure ther-

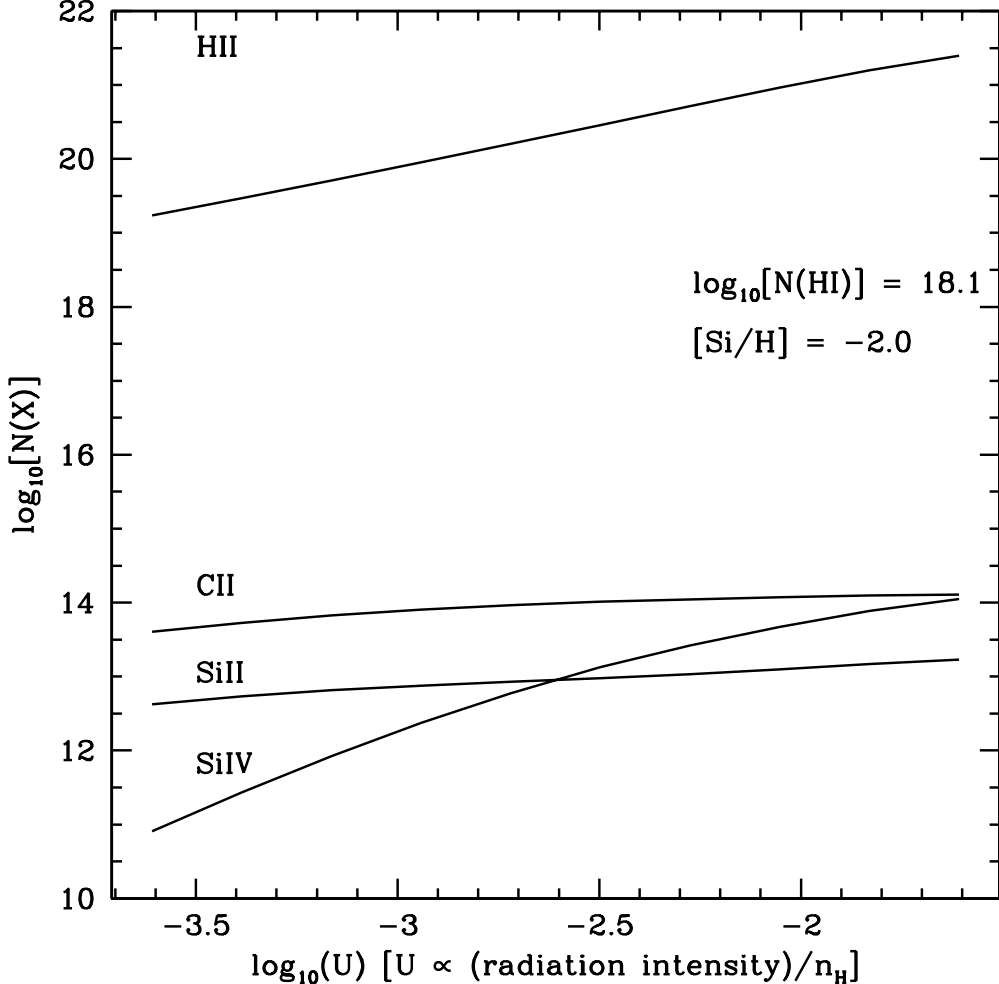


Figure 6. The ionization model generated using CLOUDY. The parameter U is defined in section 3.5.

mal broadening, assuming that the the conditions in the red component are similar to the blue component.

3.7 Are we seeing deuterium?

We expect we are seeing deuterium, for three reasons. The line we have identified as D_I occurs near the expected position for D_I, given the position of the main H_I absorptiion and the position of the Si_{II} and $\frac{3}{2}$ lines. The b parameter of the D_I line is consistent with that expected for D_I based on the fitted b parameters of the H_I component and the Si_{II} and $\frac{3}{2}$ lines. Finally, the line has a width substantially narrower than the median for forest lines, which means it is unlikely to be an H_I Ly α forest line. A metal line from another absorption system could have line width this narrow, but we know of no other absorption systems towards this quasar which have metal lines that fall at the position of the D_I line. These arguments all apply only to the bluer D_I component. We cannot independently measure the position, b parameter of column density of the the redder D_I component. However, we assume that D/H is the same in both components for the reasons given in section 3.8.

3.8 The validity of our assumption of constant D/H across different components

We assume in our models that D/H is the same for all components showing D_I. D is destroyed in star formation, so if the components have different metallicities, it is conceivable that they will also have different D/H values. Unfortunately, we cannot directly measure the metallicity of individual components due to the Ly α forest contamination around the Si_{II} and $\frac{3}{2}$ lines. However, we believe that even if the metallicity is significantly different in different components, D/H will still be very similar. Even in systems where the metallicity has been found to vary considerable between components in the same absorption system (e.g. Kirkman et al. (2003); Burles & Tytler (1998a)), the difference is rarely more than ~ 1.0 dex. Theoretical models (Fields 1996; Prantzos & Ishimaru 2001) predict that D/H remains roughly constant with metallicity until metallicities approaching 1/5 solar are reached. Since [Si/H] ~ -2.0 for this entire absorption complex (see section 3.5), we expect D/H in this absorber to be very close to the primordial value. Even if there are components with [Si/H] as high as ~ -1.0

present, we don't expect their D/H to be significantly lower than that of any lower metallicity components.

3.9 D/H in the $z=3.256$ absorber

We have the values of $N(\text{H I})$ and $N(\text{D I})$ and their errors for models (2a) - (2d), but we prefer to use an alternate method to find D/H in this absorber. Only two small regions constrain $N(\text{D I})$, and the errors on $N(\text{D I})$ are relatively large. As we saw in Crighton et al. (2003), when the errors given by VPFIT are large, it is often a sign that the χ^2 parameter space around the best fitting solution is not symmetrical. In this case the χ^2 space should be explored explicitly to find the correct error ranges.

We have generated a list of χ^2 values as a function of D/H. For each value of D/H, we fix D/H and fit the Ly α , Ly β lines and the LL, varying all other parameters to minimise χ^2 . In this case we do not fit the the total $N(\text{H I})$ and $N(\text{D I})$, since we are not interested in the errors on individual parameters, just the total χ^2 value. In this fit we tie the redshifts of each D I line to its corresponding H I line. We also tie the b parameter of the red D I component to its corresponding H I component, assuming thermal broadening, as discussed in section 3.6.

We calculate one of these graphs for an appropriate range of D/H values for each model, (2a) - (2d) (Fig. 8). The distribution of $\Delta\chi^2 \equiv \chi^2 - \chi^2_{\min}$ for each graph is the same as that of a χ^2 distribution with a number of degrees of freedom equal to the number of fixed parameters (in this case, one - D/H). Here χ^2_{\min} is the smallest value of χ^2 for a particular graph.

D/H is more tightly constrained in the cases without a floating continuum level, which is expected as there are fewer free parameters. The 3rd order continuum allows a better fit to the data than the 2nd, and is consistent with a larger D/H value. The predicted 68.3% range for D/H for the 3rd order continuum models (2b and 2d) is $1.6^{+0.25}_{-0.30} \times 10^{-5}$, with a 95.4% range of $1.6^{+0.5}_{-0.4} \times 10^{-5}$. The D/H ranges for the 2nd order continuum models are lower, $\sim 1.45 \pm 0.2 \times 10^{-5}$. Model (2b), which takes the uncertainty in the continuum level [and any effect that may have on the uncertainty in the $N(\text{H I})$ value] into account, gives the best estimate of D/H in this absorber.

4 DISCUSSION

We have identified a new Lyman limit absorption system towards PKS1937-1009, with $\log N(\text{H I}) = 18.25 \pm 0.02$ at $z = 3.256$. The Ly α and Ly β transitions are suitable for measuring D/H, and we find a 68.3% range for D/H of $1.6^{+0.25}_{-0.30} \times 10^{-5}$, and a 95.4% range of $1.6^{+0.5}_{-0.4} \times 10^{-5}$.

The metallicity of the cloud where D/H was measured is low, $[\text{Si}/\text{H}] = -2.0 \pm 0.5$. At this metallicity we expect that the D/H value will be primordial.

This value disagrees at the 99.4% level with the predicted D/H value using the Ω_b calculated from the WMAP cosmic background radiation measurements, $2.60^{+0.19}_{-0.17} \times 10^{-5}$ (Coc et al. 2004), and it exacerbates the scatter in D/H measurements around the mean D/H value. It is consistent with the D/H values measured in the ism using FUSE, [e.g., Hébrard & Moos (2003)]. However, it is not consistent with

the idea of a single primordial D/H value which stays constant until the metallicity reaches $\sim 1/10$ solar, then begins to drop off, reaching the ISM D/H at solar metallicity. Some early mechanism for deuterium astration may be the cause for the scatter in D/H values (e.g Fields et al. (2001)).

Other authors (Kirkman et al. 2003; Pettini & Bowen 2001) note that there is a trend of decreasing D/H with increasing $N(\text{H I})$ of the absorbers in which they are measured. The D/H value in this paper does not follow this trend, suggesting that the trend is not real and only due to the low number of D/H measurements.

REFERENCES

Burles S., Tytler D., 1998a, ApJ, 499, 699
 Burles S., Tytler D., 1998b, ApJ, 507, 732
 Coc A., Vangioni-Flam E., Descouvemont P., Adahchour A., Angulo C., 2004, ApJ, 600, 544
 Crighton N. H. M., Webb J. K., Carswell R. F., Lanzetta K. M., 2003, MNRAS, 345, 243
 Epstein R. I., Lattimer J. M., Schramm D. N., 1974, Nat, 263, 198
 Ferland G., 1997, Hazy, a Brief Introduction to Cloudy. University of Kentucky, Department of Physics and Astronomy Internal Report
 Fields B. D., 1996, ApJ, 456, 478
 Fields B. D., Olive K. A., Silk J., Cassé M., Vangioni-Flam E., 2001, ApJ, 563, 653
 Hébrard G., Moos H. W., 2003, ApJ, 599, 297
 Haardt F., Madau P., 1996, ApJ, 461, 20
 Kirkman D., Tytler D., Suzuki N., O'Meara J. M., Lubin D., 2003, ApJS, 149, 1
 Lanzetta K. M., McMahon R. G., Wolfe A. M., Turnshek D. A., Hazard C., Lu L., 1991, ApJS, 77, 1
 Levshakov S. A., Dessauges-Zavadsky M., D'Odorico S., Molaro P., 2002, ApJ, 565, 696
 Lu L., Sargent W. L. W., Barlow T. A., Churchill C. W., Vogt S. S., 1996, ApJS, 107, 475
 O'Meara J. M., Tytler D., Kirkman D., Suzuki N., Prochaska J. X., Lubin D., Wolfe A. M., 2001, ApJ, 552, 718
 Pettini M., Bowen D. V., 2001, ApJ, 560, 41
 Prantzos N., Ishimaru Y., 2001, A&A, 376, 751
 Sembach K. R., Wakker B. P., Tripp T. M., Richter P., Kruk J. W., Blair W. P., Moos H. W., Savage B. D., Shull J. M., York D. G., Sonneborn G., Hébrard G., Ferlet R., Vidal-Madjar A., Friedman S. D., Jenkins E. B., 2004, ApJS, 150, 387
 Spergel D. N., Verde L., Peiris H. V., Komatsu E., Nolta M. R., Bennett C. L., Halpern M., Hinshaw G., Jarosik N., Kogut A., Limon M., Meyer S. S., Page L., Tucker G. S., Weiland J. L., Wollack E., Wright E. L., 2003, ApJS, 148, 175
 Vanden Berk D. E., Richards G. T., Bauer A., Strauss M. A., Schneider D. P., Heckman T. M., York D. G., Hall P. B., Fan X., 2001, AJ, 122, 549
 Wolfe A. M., Prochaska J. X., 2000, ApJ, 545, 603

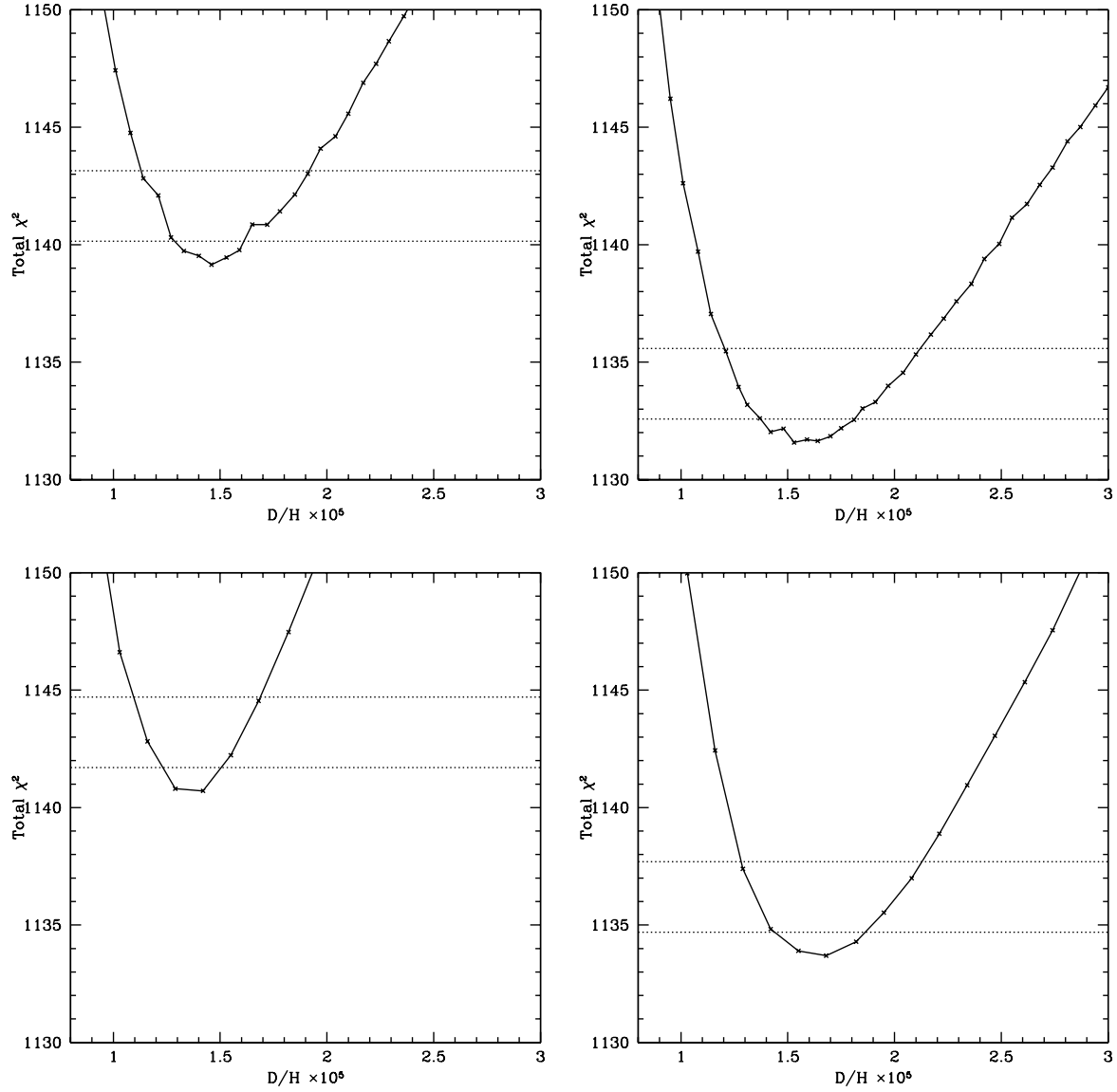


Figure 8. χ^2 vs D/H plots. The horizontal lines show the 68.3% and 95.4% confidence levels. The upper graphs are for models (2c) and (2d), where the continuum level is allowed to vary during the fit. The lower models are (2a) and (2b), where the continuum levels are fixed. The plots on the left use models with a 2nd order continuum fit over the Ly α line, the plots on the right use a 3rd order continuum.